Proceedings of the 20th International Conference on Soil Mechanics and Geotechnical Engineering– Rahman and Jaksa (Eds)

Influence of soil arching and loosening around a subsurface cavity on wave propagation

Influence de l'effet de voûte et du relâchement du sol autour d'une cavité souterraine sur la propagation des ondes

Yusuke Nakata
Taisei Corporation, 1-25-1 Nishishinjuku, Shinjuku-ku, Tokyo 163-0606, Japan, nktyus00@pub.taisei.co.jp

Umair Ali
National Engineering Services Pakistan, Pvt. Ltd., 1-C, Block-N, Model Town Extension, Lahore 54700, Pakistan

Masahide Otsubo & Reiko Kuwano
Institute of Industrial Science (IIS), The University of Tokyo, 4-6-1 Komaba, Meguro-ku, Tokyo 153-8505, Japan

ABSTRACT: Subsurface cavities, often observed around deteriorated buried pipes, potentially cause sinkholes or road cave-ins. Ground-penetrating radar method has been utilized to detect subsurface cavities, whereas dynamic wave surveys including surface or downhole wave surveys still need more research and experiences to be an alternative measure. In this study, reduced scale model tests are conducted to understand the influence of cavity on stress wave velocities using piezoelectric transducers. To understand micromechanics of wave propagation around a cavity, discrete element method (DEM) is adopted considering inter-particle suction and tension forces. Both model tests and DEM results agree that both compression (P-) and shear (S-) waves deaccelerate in the vicinity of a cavity due to the loosening of soil where the number of contacts per particle drops. DEM analyses reveal that P-waves propagate faster along the direction of soil arching, whereas S-wave propagation is less sensitive to the presence of soil arching. Further, DEM results suggest that velocity tomography that can be obtained from in-situ dynamic wave surveys can possibly be an alternative method to find a subsurface cavity.

RÉSUMÉ : Les cavités souterraines peuvent causer des fontis en surface. La méthode de radar à pénétration de sol est utilisée pour détecter les cavités souterraines, mais les études par propagation d'ondes sismiques, consistant à détecter les ondes de surface ou de volume, pourraient constituer une méthode de détection alternative. Dans cette étude, des essais sur modèle à échelle réduite sont menés pour comprendre l'influence d'une cavité sur les vitesses de propagation des ondes sismiques à l'aide de capteurs piézoélectriques. Pour comprendre les phénomènes micromécaniques, la méthode par éléments discrets (DEM) est utilisée en parallèle. Les essais sur le modèle et les résultats de l'étude par éléments discrets ont tous deux montré que les ondes de compression P et de cisaillement S se propageant à proximité d'une cavité sont ralenties puisque le nombre de contacts entre particules chute à proximité de la cavité. Les études par éléments discrets révèlent que les ondes P se propagent plus rapidement le long de la voûte du sol, les ondes S y sont par contre moins sensibles. Des analyses plus poussées montrent que la tomographie par ondes dynamiques peut être une méthode alternative pour trouver une cavité souterraine.

KEYWORDS: Wave propagation; subsurface cavity; soil arching; discrete element method; granular material.

1 INTRODUCTION

The number of road cave-in cases associated with deterioration of buried infrastructure, such as breakage of pipelines, reaches several thousand cases annually in Japan. Subsurface cavities grow underground and often lead to a sudden collapse of the ground surface. As a countermeasure, the ground-penetrating radar method has been utilized to detect subsurface cavities in practice. However, its applicability is limited to the relatively shallow ground, for example, 1.5m depth from the ground surface. Thus, alternative methods are required to overcome this limitation. In contrast, to the authors' knowledge, there is no such a report that dynamic wave surveys including surface and down-hole wave surveys successfully detected the precise location of subsurface cavities. Kuwano et al. (2018) found in laboratory model tests that soil surrounding a subsurface cavity becomes loosened, whereas an arch is created over the cavity to support the upper ground. However, the micromechanics of the stress transmission in such a complex condition remains unclear.

This study aims to understand the characteristics of elastic wave propagation around a subsurface cavity considering both soil arching and loosening and discuss whether the dynamic wave survey can detect the presence of a cavity. Both laboratory model tests and discrete element method (DEM) simulations are conducted to answer the above question.

2 MODEL TEST

Uniformly graded silica sand having a median particle diameter of 0.5mm was used to prepare the model ground in a cylindrical chamber with a diameter of 0.3m (Fig. 1). The air-dry sand was pluviated from a specific elevation to achieve a specimen height of 0.2m with a relative density of 50%. Two pairs of planar piezoelectric transducers were placed on the base and top surface of the ground (Fig. 1). Following an experimental approach detailed in Kuwano et al. (2018), pore water was supplied from two holes in the base and discharged together with soil from a center hole in the base having a diameter of 5mm. As a result, a cavity was generated above the center hole. The remaining ground was kept at partially saturated conditions.

P- and S-waves propagating downwards were measured by

transmitting waves from the top surface and receiving at the base (Fig. 1) at three different conditions: before generating a cavity (no cavity), after generating a small cavity (small cavity), and after enlarging the size of the cavity due to second discharge (large cavity). Planar piezoelectric transducers (Dutta et al. 2019) and bender elements (Shirley & Hampton 1978) were used for measuring P-waves and S-waves, respectively (Fig. 2). A thin coating of epoxy resin was applied to the surface of the elements to prevent damage due to water and abrasion caused by angular sand grains. The elements were placed inside acrylic frames (Fig. 2) and supported using silicone and epoxy resin. A uniform load of about 2.7kPa was applied on the surface of the sandy ground to ensure firm contact between the sand grains and the transducers (refer to Nakata (2020) for more details about the experimental method).

A single period of a sinusoidal wave having a frequency of 5kHz and a double amplitude voltage of 140V was inserted from the transmitter. Fig. 3 compares both P- and S-wave signals received at the base for the three test conditions. The vertical axis is the transmitted or received voltage normalized by their maximum amplitudes for "no cavity" case. Fig. 3 depicts that both P- and S-waves travel slower after a cavity is generated. Similarly, the amplitude of received signals is also reduced due to the influence of the cavity.

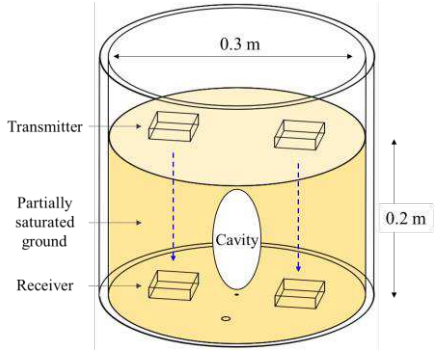

Figure 1. Schematic of model test ground with a cavity.

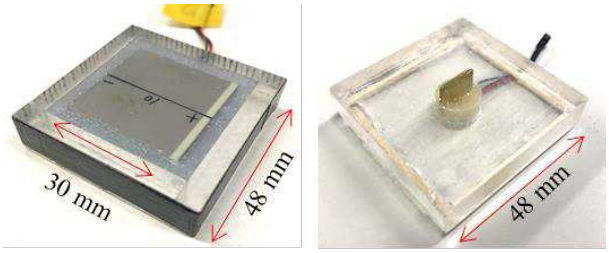

Figure 2. Piezoelectric transducers (left) planar element to measure P-wave signals and (right) bender element to measure S-wave signals.

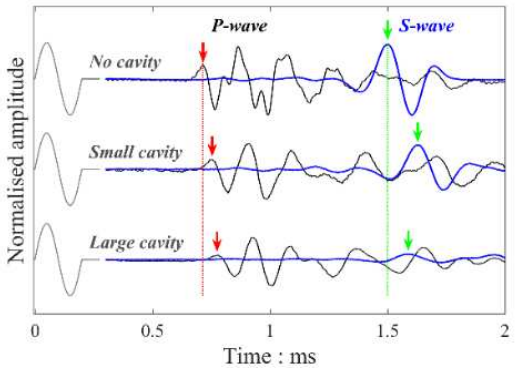

Figure 3. Elastic wave signals observed in laboratory model tests.

3 DEM SIMULATION PROCEDURE

It was difficult to study the micromechanics of elastic wave propagation based on the laboratory model tests. Therefore, DEM simulations were performed to study how elastic waves propagate around a cavity associated with the development of soil arching. The present DEM analyses focus on two-dimensional wave propagation characteristics using a rectangular container to simplify the complicated three-dimensional wave propagation in the model tests.

3.1 *Contact model for unsaturated soil*

It is not easy to model the unsaturated soil behavior using DEM. Some research groups proposed contact models that consider capillary actions (e.g. Farouk et al. 2004; Ji-Peng et al. 2017; Monnet et al. 2019). In this study, a new suction-tension contact model was implemented in the open-source LAMMPS (Plimpton 1995), and details of its derivation process are given in Ali et al. (2019). The adopted contact model considers capillary forces acting between two particles as well as Hertz-Mindlin contact model (Johnson 1985). The capillary force (F_c) is given as:

$$F_c = \pi b' T_c \left[\frac{b'}{R}\left(\frac{1}{sec\theta - 1} - \frac{1}{tan\theta + 1 - sec\theta}\right) + 2\right] \quad (1)$$

where T_c is the surface tension of pore water; R, b, b' and θ are the geometric constants illustrated in Fig. 4. Referring to Ali (2020), the b, b' and θ parameters are calculated automatically depending on the degree of saturation (S_r), particle radius (R) and overlap (or separation) (δ) between two particles.

The capillary force (F_c) is summed up with the non-linear repulsive force based on the Hertz-Mindlin model. Fig. 5 shows the schematic of the force-overlap/separation relationship between two particles. It should be noted that the F_c value in Eq. 1 is applicable when two particles are in contact (i.e. $\delta > 0$). The capillary force is considered to decline as the distance between the two particles increases following a quadratic function (Fig. 5). The rapture distance of the capillary bridge is difficult to measure precisely; this is assumed to occur at $\delta = -1\mu m$. The capillary force is assumed to act in the normal contact, but the tangential contact follows the simplified Hertz-Mindlin model with a binary coulomb friction limit.

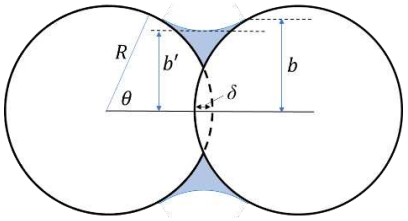

Figure 4. Schematic of capillary bridge between two particles.

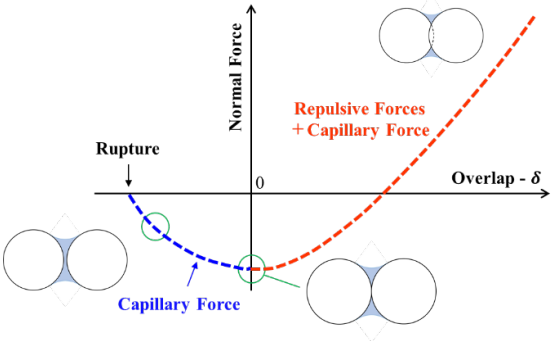

Figure 5. Schematic of the force-displacement relationship between two particles for normal contact interaction.

3.2 *Preparation of DEM model ground*

Typical glass bead properties were adopted (Young's modulus: 71.6GPa, Poisson's ratio: 0.23, and specific gravity: 2.5). The diameters of spherical particles range from 1.2mm to 2.2mm, representing a uniformly graded soil.

To represent the ground preparation method in the model test, air-pluviation in a dry condition was adopted. The model ground having 0.4m in length (X), 0.2m in height (Z), and 0.02m in depth (Y) was prepared in 10 layers (Fig. 6). The base was rigid wall boundary, while periodic boundaries were used in the horizontal (X and Y) directions. The use of periodic boundaries in the horizontal direction to discuss the development of soil arching was justified in Ali et al. (2020). The DEM model ground is wider than the laboratory case to reduce the effect of side boundaries. To prepare a dense ground, the interparticle friction was set to zero during the pluviation process. The model ground consists of 360,170 spherical particles with a void ratio of 0.61. Fig. 6 displays the contact force chains connecting the centroids of particles in contact (see inset figure) where the top 5% of large forces at each elevation are shown. After the ground became stable with the application of viscous and local damping, the interparticle friction was increased to 0.35.

Considering the size and shape of the cavity observed in the model test (Nakata 2020), particles inside the space of the cavity were deleted from the DEM model ground (Fig. 7). Simultaneously, S_r was increased to 7.35% uniformly in the entire ground. In this process, the mass of pore water was considered by adding equivalent mass to each particle. When T_c = 0.0728 N/m (value for water at 20°C) was adopted, the ground deformed unstably due to relatively low F_c compared to the weight of individual particles. Note that larger particles were used in DEM compared to the model test, which caused this instability. To hold the model ground with a subsurface cavity stably, T_c was increased artificially by a factor of 20.

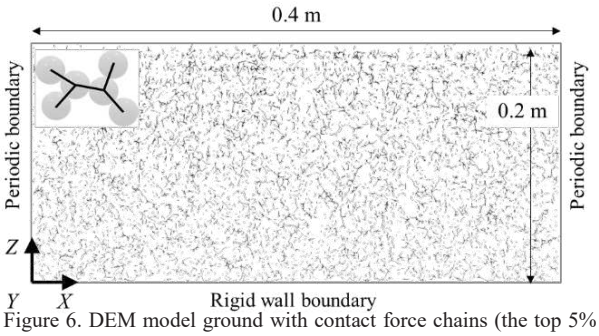

Figure 6. DEM model ground with contact force chains (the top 5% of large forces at each elevation are shown).

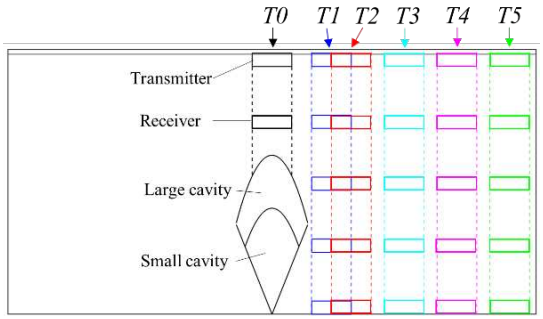

Figure 7. Size and shape of cavity and locations of transmitters and receivers for wave measurements.

4 GROUND DEFORMATION AND FORCE CHAINS

Fig. 8 displays the ground deformation (vertical displacement) due to the generation of a small cavity where the displacement is magnified by a factor of 10 for better visibility. Fig. 8 also shows soil arching developed over the cavity. The model ground is loosened inside the soil arch as indicated by the light-blue color. The maximum settlement of the ground is around 1.6mm, which is close to the median particle size.

The total normal contact force shown in Fig. 8 can be decomposed into the repulsive force and capillary force, and they are depicted in Fig. 9 and Fig. 10, respectively. From Fig.9, in comparison with Fig. 6, soil arching is developed in a similar pattern reported in Ali et al. (2020) for trapdoor conditions. Ali et al. (2019) quantified change in fabric tensor after generating a rectangular-shaped cavity. In Fig. 10, capillary forces are distributed randomly but uniformly. It should be noted that the soil arching is not evident very close to the cavity due to the loosening of the ground (Fig. 9). This suggests that the soil grains in the vicinity of the cavity do not contribute to the stability of the ground but are rather held by the capillary forces.

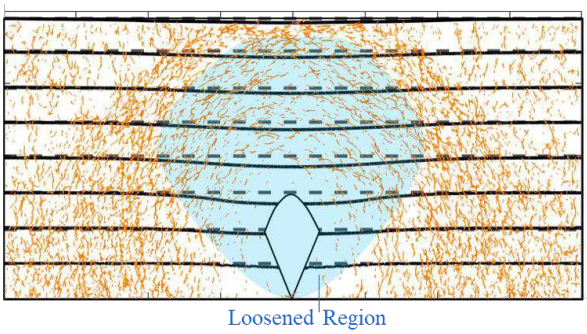

Figure 8. Ground deformation (vertical displacement) due to the generation of a small cavity and soil arching formed over the cavity. The light-blue color indicates the loosened region of the model ground.

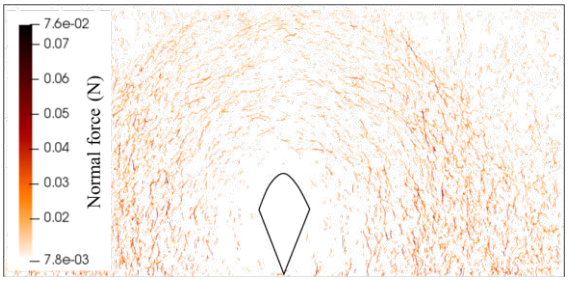

Figure 9. Distribution of repulsive forces after generating a small cavity (the top 5% of large forces at each elevation are shown).

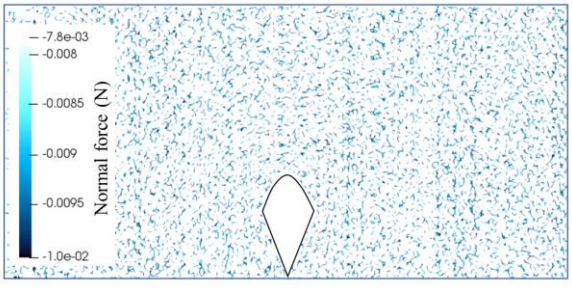

Figure 10. Distribution of capillary forces (F_c) in DEM model ground after generating a small cavity (negative sign corresponds to the attractive forces).

5 WAVE PROPAGATION SIMULATIONS

Transmitters are located on the ground surface having a region of 30mm in length (X), 10mm in height (Z), and 20mm in depth (Y) (Fig. 7). The particles inside the region of each transmitter were excited in Z- or Y-direction to generate P- or S-waves, respectively, with a single period of cosine wave form (double amplitude displacement: 100nm; frequency: 10kHz). Neither local nor viscous damping was used during wave propagation.

Fig. 11 shows a snapshot of P-wave propagation in the model ground without any cavity. The color bar indicates the absolute velocity of individual particles at 0.48ms after exciting transmitter *T0*. The wavefront spreads concentrically but faster slightly in the downward direction as the increased confining stress in the deeper ground leads to a larger wave velocity. Besides, the waves propagating in the horizontal direction seem coupled with S-wave motions in a complicated manner.

Fig. 12 shows a snapshot of P-wave propagation in the model ground with a small cavity when the entire surface is excited simultaneously. The continuous lines show the wavefronts at selected elapsed times after the excitation where a snapshot of propagating waves at 0.36ms is overlaid. P-waves propagate slowly inside the soil arch (Fig. 8). At $X = 0$ and 0.4m (see Fig. 6), the fastest P-waves are observed, where the arrival time to the base was almost identical to that without any cavity.

In the model test, the locations of the transmitters were about 20mm off the side edge of the cavity (Fig. 7), and a similar condition was reproduced by exciting transmitter *T2* in DEM. P- and S-wave propagation patterns are visualized in Fig. 13 and Fig. 14, respectively. Regarding P-waves, the wavefront appears normal to the direction of the arch, i.e. P-waves propagate faster along the direction of the arch. In Fig. 14, the S-wave velocity is lower than the P-wave velocity, as expected. Contrary to P-waves, the pattern of S-wave propagation is not very sensitive to the direction of the soil arch. Dutta et al. (2020) and Li et al. (2021) found that S-wave velocity (V_s) reduces when the mean coordination number, CN (number of contacts per particle) drops, whereas P-wave velocity (V_p) is influenced by both CN and the stress along its propagation direction, based on DEM analyses.

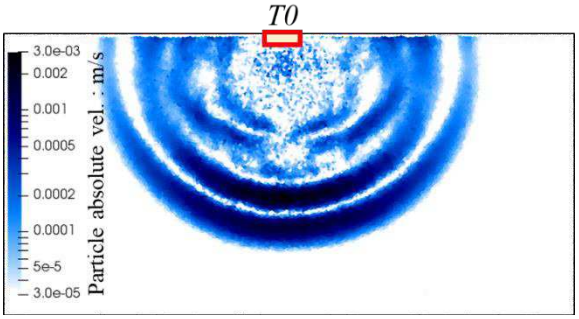

Figure 11. P-wave propagation in DEM model ground without cavity when transmitter *T0* is excited vertically.

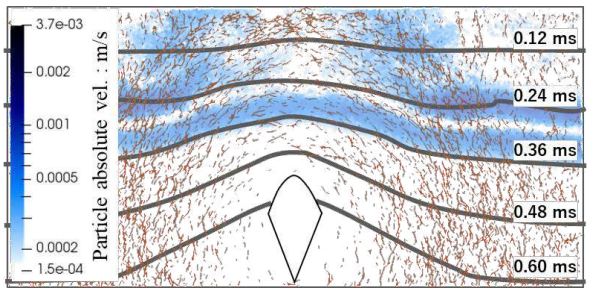

Figure 12. P-wave propagation in DEM model ground with a small cavity when the entire surface is excited vertically.

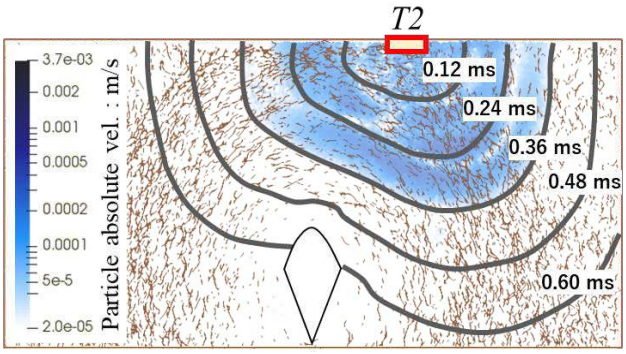

Figure 13. P-wave propagation in DEM model ground with a small cavity when transmitter *T2* is excited vertically.

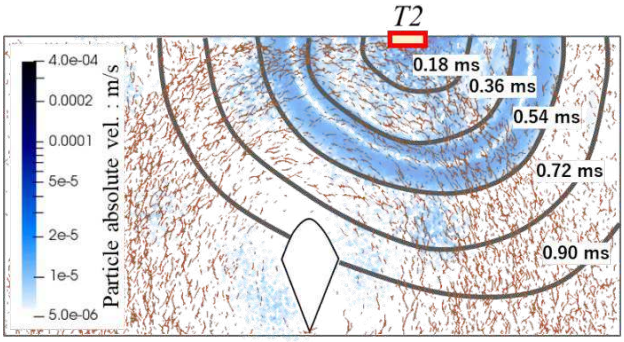

Figure 14. S-wave propagation in DEM model ground with a small cavity when transmitter *T2* is excited horizontally in the *Y*-direction.

Fig. 15 illustrates the spatial variation of changes in CN due to the generation of the small cavity. The reduction in CN is observed in a wide region, even outside of the soil arch towards the top surface. The reduction in CN seems to impact significantly on V_s as well as the formation of soil arch.

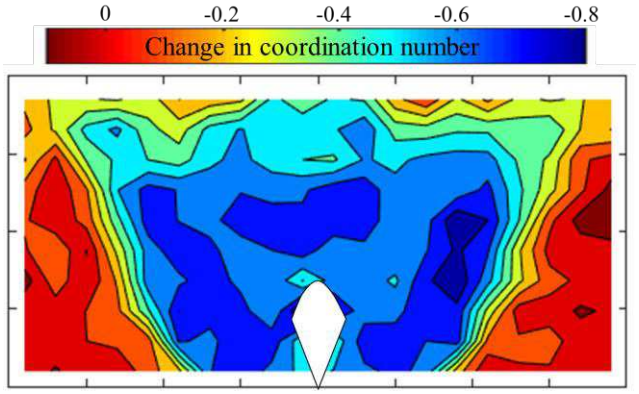

Fig. 15. Change in coordination number (number of contacts per particle) in DEM model ground due to the generation of a small cavity.

6 VELOCITY TOMOGRAPHY TO DETECT A CAVITY

Section 5 has investigated how elastic waves propagate around a subsurface cavity, focusing on the motion of individual particles. However, such an approach cannot be compared with the results, in neither laboratory model tests nor in-situ measurements. In this section, in-situ measurement approaches, such as the down-hole or cross-hole method (Clayton 2011) were considered to better compare DEM data with field measurement data. Here, the down-hole measurement method was adopted and waves propagating downwards were analyzed using multiple receivers

(groups of particles). Referring to Fig. 7, transmitters *T0* to *T5* were excited individually, and the received signals (displacement of particles) at the four receivers along each measurement line (only one along the *T0* measurement line) were processed to find V_p and V_s from the time-domain signals at each receiver locations. To determine the arrival of waves, the first peaks of the signals were selected as detailed in Li et al. (2021). Using wave velocity data at 21 locations for the half side of the model ground (Fig. 7), two-dimensional velocity tomography was obtained.

Fig. 16 shows the spatial contour of changes in V_p due to the generation of a small cavity (left side) or large cavity (right side). The dark-blue color indicates a reduction in V_p observed above the cavity towards the top surface, while the light-yellow color indicates an increase in V_p observed near the base. The V_p contour changes normal to the direction of the soil arch in Fig. 16, both for small and large cavity cases.

Fig. 17 compares V_p and V_s tomography results for the DEM model ground with a small cavity. The V_s tomography shows a wider range of reduction in V_s even near to the base around the cavity. The reduction pattern in V_s appears similar to that in *CN* (Fig. 15), indicating a stronger correlation between V_s and *CN*, than V_p and *CN*. These results are in line with the particle-scale analyses of wave propagation presented in Figs. 12 to 14. Therefore, this suggests that the down-hole survey method can potentially be used to detect a subsurface cavity in practice.

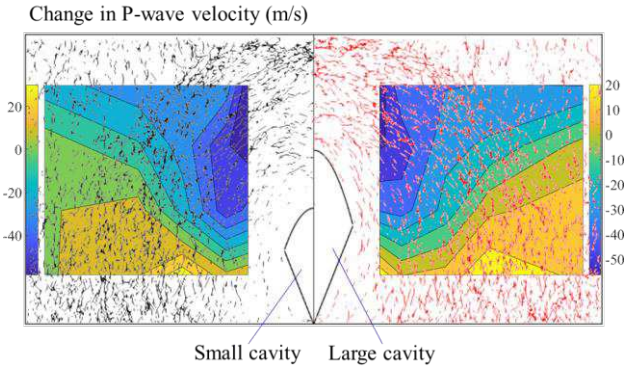

Fig. 16. Change in P-wave velocity tomography due to generation of small cavity (left half) and large cavity (right half) in DEM model ground.

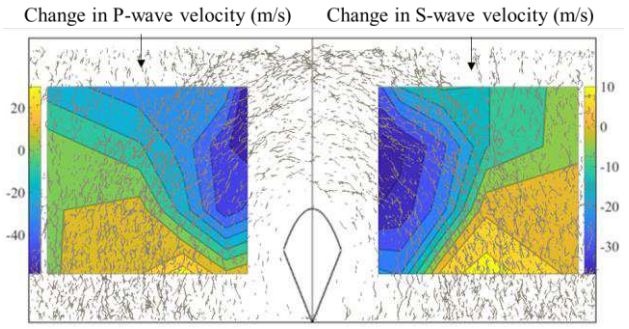

Fig. 17. Change in velocity tomography due to generation of small cavity for P-waves (left half) and S-waves (right half) in DEM model ground.

7 CONCLUSIONS

This study has investigated the characteristics of wave propagation around a subsurface cavity using both laboratory model tests and DEM simulations. Although direct comparison between the two approaches was limited, qualitative analyses on the observed results can lead to the following main conclusions.

- Both the laboratory model tests and DEM simulations adopted here agree to show a reduction in wave velocities (both V_p and V_s) around a subsurface cavity.
- DEM data revealed that a loosened region appears inside the soil arch where the coordination number drops unstably but the capillary force holds the loosened ground stably.
- P-wave propagation pattern is affected by a combined effect of weakened soil structure and soil arching, while the effect of weakened soil structure largely influences S-wave propagation pattern compared with the effect of soil arching.
- Using existing geophysical testing methods, such as down-hole or cross-hole survey, can potentially provide velocity tomography influenced by subsurface cavities and contribute to detect them with an advanced interpretation.

8 ACKNOWLEDGEMENTS

This work was supported by JSPS KAKENHI Grant Number 19K15084. The simulations presented in this contribution were conducted using the Fujitsu PRIMERGY CX600M1/CX1640M1 (Oakforest-PACS) in the Information Technology Center, The University of Tokyo.

9 REFERENCES

Ali U., Otsubo M. and Kuwano R. 2019. Suction-Tension model for verifying ground cavity formation using discrete element method. *Proc. 15th Int'l Conf. on Geotechnical Engineering,* Lahore, 306-313.

Ali U., Otsubo M., Ebizuka H. and Kuwano R. 2020. Particle-scale insight into soil arching under trapdoor condition. *Soils and Foundations* 60 (5), 1171-1188.

Ali U. 2020. *Experimental and numerical analyses of soil arching and stability mechanism under trapdoor and underground cavity conditions*, Ph.D. thesis, The University of Tokyo.

Clayton C.R.I. 2011. Stiffness at small strain: research and practice. *Géotechnique* 61 (1), 5-37.

Dutta T.T., Otsubo M., Kuwano R. and O'Sullivan C. 2020. Evolution of shear wave velocity during triaxial compression. *Soils and Foundations* 60 (6), 1357-1370.

Dutta T.T., Otsubo M., Kuwano R. and O'Sullivan C. 2019. Stress wave velocity in soils: Apparent grain-size effect and optimum input frequencies. *Géotechnique Letters* 9 (4), 340-347.

Farouk A., Lamboj L. and Kos, J. 2004. A numerical model to predict matric suction inside unsaturated soils. *Acta Polytechnica*, 44 (4), 3-10.

Ji-Peng W., Xia L. and Hai-Sui Y. 2017. Stress-force-fabric relationship for unsaturated granular materials in pendular states. *Journal of Engineering Mechanics*, 143 (9), 4017068.

Johnson, K.L. 1985. *Contact mechanics*. Cambridge University, Cambridge, U.K.

Kuwano R., Sera R. and Ohara Y. 2018. Model tests to simulate formation and expansion of subsurface cavities. *Proc. 9th Int'l Conf. on Physical Modelling in Geotechnics*, London, 1087-1092.

Li Y., Otsubo M. and Kuwano R. 2021. DEM analysis on the stress wave response of spherical particle assemblies under triaxial compression. *Computers and Geotechnics* 133, 104043.

Monnet J., Mahmutovic D., Boutonnier L. and Taïbi S. 2019. A theoretical retention model for unsaturated uniform soils. *European Journal of Environmental and Civil Engineering*, 23 (3), 345-367.

Nakata Y. 2020. *Stress transmission around an underground cavity evaluated using elastic waves*, Master's thesis, The Univ. of Tokyo.

Plimpton S. 1995. Fast parallel algorithms for short-range molecular-dynamics. *Journal of Computational Physics* 117 (1), 1-19.

Shirley D. and Hampton L. 1978. Shear-wave measurements in laboratory sediments. *J. Acoustical Soc. Am.* 63 (22), 607-613.